Determination of plasma pinch time and effective current radius of double planar wire array implosions from current measurements on a 1-MA linear transformer driver

Adam M. Steiner,[1] David A. Yager-Elorriaga,[1] Sonal G. Patel,[1] Nicholas M. Jordan,[1] Ronald M. Gilgenbach,[1] Alla S. Safronova,[2] Victor L. Kantsyrev,[2] Veronica V. Shlyaptseva,[2] Ishor Shrestha,[2] and Maximillian T. Schmidt-Petersen[2]
[1]*Plasma, Pulsed Power, and Microwave Laboratory, Department of Nuclear Engineering and Radiological Sciences, University of Michigan, Ann Arbor, Michigan 48109, USA*
[2]*Department of Physics, University of Nevada, Reno, Nevada 89557, USA*

(Received 1 June 2016; accepted 22 August 2016; published online 20 October 2016)

Implosions of planar wire arrays were performed on the Michigan Accelerator for Inductive Z-pinch Experiments, a linear transformer driver (LTD) at the University of Michigan. These experiments were characterized by lower than expected peak currents and significantly longer risetimes compared to studies performed on higher impedance machines. A circuit analysis showed that the load inductance has a significant impact on the current output due to the comparatively low impedance of the driver; the long risetimes were also attributed to high variability in LTD switch closing times. A circuit model accounting for these effects was employed to measure changes in load inductance as a function of time to determine plasma pinch timing and calculate a minimum effective current-carrying radius. These calculations showed good agreement with available shadowgraphy and x-ray diode measurements. *Published by AIP Publishing.*
[http://dx.doi.org/10.1063/1.4965241]

I. INTRODUCTION

The linear transformer driver (LTD) is a compact pulsed power technology that has recently received attention as an alternative to the conventionally used Marx-driven accelerator.[1–4] The smaller footprint and fast risetimes without pulse shaping make it an attractive technology for constructing next generation pulsed power machines,[5] such as the proposed Z-300 and Z-800 experiments at Sandia National Laboratories.[6] A recent publication[7] explored the dynamics of planar wire array (PWA) experiments on the Michigan Accelerator for Inductive Z-Pinch Experiments (MAIZE), a single-cavity LTD at the University of Michigan. Current-driven wire array implosions have been studied in various geometries[8–10] as sources of high-energy x-rays on various MA-scale pulsed power machines. Recently, PWAs have been studied in detail on the Zebra generator,[10–20] which produces ∼1 MA in 100 ns risetime with 1.9 Ω driver impedance, and on the Saturn driver at Sandia.[21] The joint University of Nevada, Reno/University of Michigan campaigns[7] were the first planar wire array studies performed on a linear transformer driver.

The PWA campaigns on MAIZE demonstrated substantial dependence of current magnitude and risetime on load inductance, a behavior not observed during previous experiments on higher impedance drivers.[10–20] In this work, we will discuss this load dependence in greater detail as well as demonstrate a method for determining load inductance from a measurement of current. A measurement of time-dependent load inductance change provides information on when significant mass redistribution occurs during the pinch process and can also be used to calculate an effective current-carrying radius of the imploding plasma. Previous measurements of inductance obtained from simultaneous voltage and current measurements on wire array implosions on Z[22] were able to obtain these insights on the timing of wire core motion. Additionally, voltage and current measurements of gas puff Z-pinches on Saturn were used to calculate time-dependent inductance and energy coupled into the load, assuming negligible load resistance.[23,24] Due to the relative simplicity of the single-stage LTD current driver circuit, a full circuit model can be implemented, using the charging voltage as an initial condition, to enable a measurement of load inductance requiring *only* a current measurement.

The experimental setup for double planar wire array (DPWA) experiments on MAIZE is detailed in Section II. In Section III, a circuit model for the LTD is presented and used to estimate risetime and peak current for a variety of load parameters. It will be shown in Section IV that during the DPWA experiments, the switches in the LTD did not fire simultaneously and exhibited firing time variation of several hundred ns. This effect requires the implementation of a circuit model with each LTD brick (where a brick consists of two capacitors and one spark-gap switch) having its own triggering time to accurately model the current output and calculate the load inductance as a function of time. In Section V, calculations of inductance and minimum effective current carrying radius using the circuit model are shown; these inductance measurements are compared with measurements from other diagnostics.

II. EXPERIMENTAL CONFIGURATION

The MAIZE facility consists of a single-stage 0.1 Ω LTD capable of driving 1 MA with 100 ns risetime into a matched, non-inductive load. A vacuum chamber 1 m in diameter is positioned inside the driver to house the load and associated diagnostics.[3] The driver section is directly

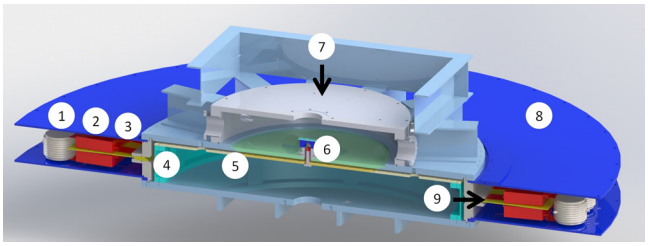

FIG. 1. Three dimensional model of the assembled MAIZE LTD. (1) Spark gap switch; (2) 40 nF capacitor; (3) iron core region (core not pictured); (4) coaxial transmission line section; (5) radial transmission line section; (6) load region; (7) vacuum chamber; (8) oil chamber; (9) high voltage insulator.

connected to the load through a coaxial-to-radial magnetically insulated transmission line (MITL). A cutaway schematic view of the fully assembled MAIZE is shown in Figure 1. More details of single-stage LTD operation and the MAIZE facility are available in other publications.[1–3,25–27]

The experimental configuration used in the DPWA implosions is shown in Figure 2. For the shots treated in this paper, the load consisted of two sets of six 5.1 μm stainless steel 304 wires spanning an AK gap of 9 mm with the total load mass of 19.4 μg. The distance between wires in the same plane, referred to as the interwire spacing, was 1 mm, and the distance between wire planes, referred to as the intergap spacing, was varied between 3 mm and 6 mm. Figure 3 shows a closeup view of a DPWA load. This load region was connected to the radial MITL by a coaxial adapter hardware section that replaced the triplate transmission line used in previous experiments.[25,26] The total inductance of the load region including this adapter was calculated from a magnetostatic simulation performed in ANSYS Maxwell and was found to be approximately 18 nH.

Current measurements are obtained by averaging signals from four B-dot probes located azimuthally symmetrically at a radial position of approximately 0.4 m from the center of the load region; a fifth B-dot probe located at a radial position of approximately 0.35 m was also fielded for some of the shots. The estimated uncertainty of each B-dot obtained from repeated current measurements into a constant resistive load

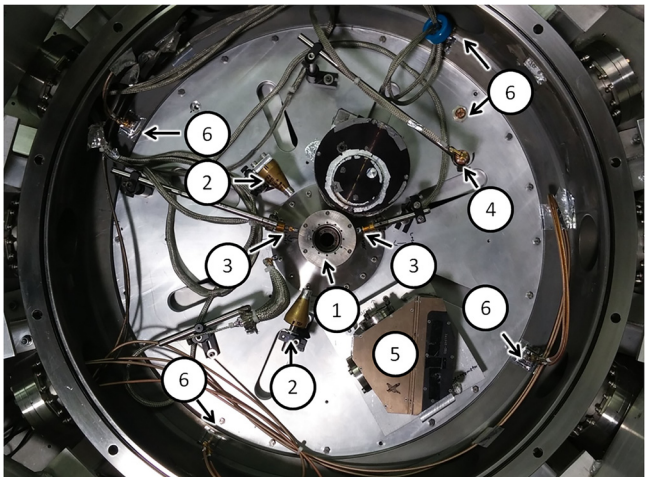

FIG. 2. MAIZE vacuum chamber top down view with load hardware and diagnostics. (1) Load hardware adapter; (2) pinhole camera with x-ray film; (3) X-ray diode; (4) Faraday cup (in loading position); (5) KAP x-ray spectrometer; (6) differential B-dot current probe.

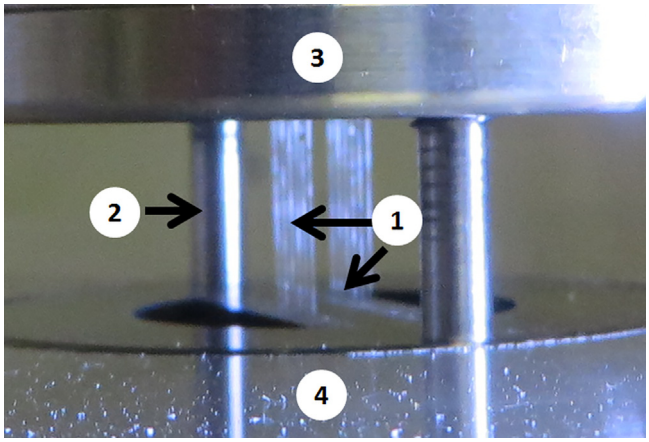

FIG. 3. Close up isometric view of load region for DPWA experiment. (1) Planar array conisisting of six 5.1 μm-diameter 304 SS wires; (2) two supporting rods that are removed during installation prior to the shot; (3) cathode; (4) anode.

is 5%, so averaging all four B-dots measures the current with an error of approximately 2.5%. A 532 nm, 2 ns, frequency-doubled Nd:YAG pulse is split into four beams with approximately 1.3° of angular separation between adjacent beampaths to obtain the four-frame shadowgraphy of the wire ablations with approximately 10 ns between frames. Time-dependent X-ray emission is monitored by three AXUV-HS-5 x-ray diodes (0.7 ns time resolution) with filters of cutoff energies 1.4 keV, 3.5 keV, and 9 keV. Additional diagnostics fielded in these experiments, which were part of the second collaborative UNR-UM campaign, are described in Ref. 7.

III. STANDARD OPERATION MAIZE CIRCUIT MODEL

Figure 4 shows the simplified LTD circuit model used to represent MAIZE. This circuit is similar to the one used to model single-stage LTDs at Sandia National Labs,[1,2,27] accounting for the effect of the iron cores as an approximately constant equivalent resistance in parallel with the load,[28] and including the spatially dependent impedance of the transmission line as a series of discrete transmission line elements. Taking the assumption that all switches are triggered simultaneously, the capacitors and switches are lumped together into a driver-side equivalent resistance (Rgen = 16.5 mΩ), inductance (Lgen = 6.0 nH), and capacitance (Cgen = 0.800 μF). The equivalent core resistance has in general been observed to change as a function of machine age; at the time of these experiments Rcore = 0.9 Ω. The impact of the transmission

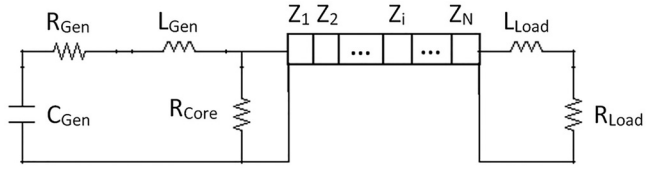

FIG. 4. Schematic of LTD circuit. R_{gen}, L_{gen}, and C_{gen} refer to the lumped resistance, inductance, and capacitance of the 40 parallel bricks, respectively. R_{core} refers to the parallel resistance of the iron cores due to eddy currents, which dominates core behavior provided magnetic saturation is not reached. L_{load} and R_{load} are the inductance and resistance of the load, respectively. The transmission line is represented as N discrete elements, each with characteristic impedance Z_i.

line usually cannot be neglected because the integral impedance of the transmission line is on the order of the impedance of the driver and can even exceed the impedance of the driver if the load hardware is designed to join with the radial transmission line at a small radius.

When the charging voltage is specified as an initial condition on the equivalent capacitance of the driver, the system of equations governing voltage and current at each circuit element is closed for a given set of load parameters. These equations are Kirchoff's current and voltage laws, the voltage-current relations for capacitive, resistive, and inductive elements, and the telegrapher's equations for a radial transmission line

$$\frac{\partial V}{\partial r} = -L' \frac{\partial I}{\partial t} = -\frac{\mu_0 h}{2\pi r} \frac{\partial I}{\partial t}, \tag{1}$$

$$\frac{\partial I}{\partial r} = -C' \frac{\partial V}{\partial t} = -\frac{2\epsilon_0 \pi r}{h} \frac{\partial V}{\partial t}, \tag{2}$$

where V is the voltage, I is the current, L' and C' are the inductance and capacitance per unit length of the radial transmission line, respectively, r is the radial position, h is the gap height, and μ_o and ε_o are the permeability and permittivity of free space, respectively. The system of equations is solved numerically, using backwards time differencing for numerical stability, in the form of the equation

$$A\phi_{n+1} = \phi_n, \tag{3}$$

where ϕ_n is a vector storing all of the nondimensionalized voltages and currents at timestep n and A is a matrix representing the discretized telegrapher's equations, Kirchoff's laws, and the relations

$$V_{n+1} = \frac{L(I_{n+1} - I_n)}{\Delta t}, \tag{4}$$

$$I_{n+1} = \frac{C(V_{n+1} - V_n)}{\Delta t}, \tag{5}$$

$$V_{n+1} = RI_{n+1}, \tag{6}$$

for inductive, capacitive, and resistive elements, respectively.

In the above analysis, L_{Load} and R_{load} are taken to be constant with time, and the nondimensionalized values stored in ϕ are currents and voltages, which are solved for as a function of time. In the limit that the impedance of the load is inductance-dominated, as is often the case in z-pinch plasmas, time-dependent load inductance can be calculated from a measurement of current. To accomplish this, the measured current is replaced by the nondimensionalized load inductance in ϕ, and A becomes time-dependent to represent the inclusion of known, time-dependent current. Solving (3) then gives the voltage and current at all other points in the system along with the time-dependent values L_{Load}. This method is also valid if a suitable time-averaged resistance R_{load} is included, provided changes in load impedance are dominated by changes in inductance.

Figure 5 shows a current trace generated by the circuit model along with a measured current trace on a static resistive load with the known resistance of 80 mΩ and the inductance of 12 nH. The measurement demonstrates agreement well within the nominal 2.5% error on the B-dot probes, which allows the inductance changes on the order of 0.5 nH to be

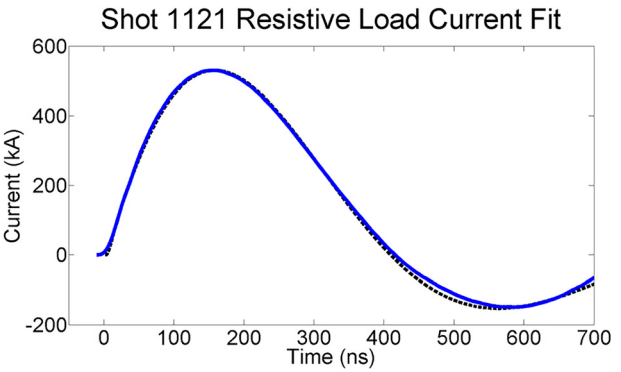

FIG. 5. Comparison of measured current (solid curve) and simulated current (dashed curve) for a static load. The prediction agrees nearly exactly with the measurement until around 350 ns (well after peak current), after which point charge buildup on the surface of the B-dot sensors impacts their accuracy.

resolved with this method. On most dynamic load shots, the B-dot probes acquire a spurious signal starting at around 350–400 ns; this spurious signal always occurs well past peak current and is attributed to charge buildup on the surface of the B-dot sensors after the voltage has changed signs.

A parameter sweep of simulated peak current and risetime as functions of time-averaged load resistance and inductance is shown in Figure 6. The load inductances on this

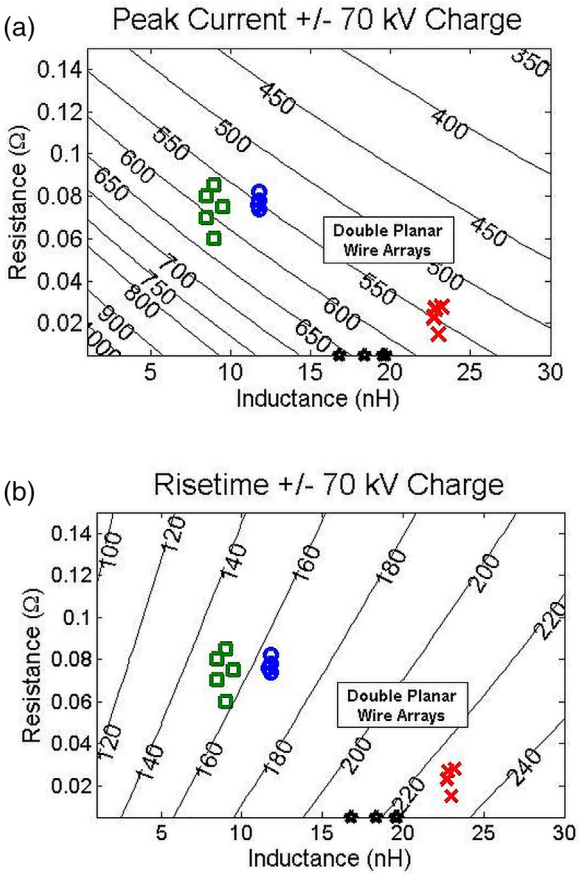

FIG. 6. Results from load parameter sweep showing (a) peak current in kiloamps and (b) risetime in nanoseconds at the load. Observed parameters from a sample of MAIZE shots are indicated as follows: Planar foil[25] (green square) cylindrical liner[26] (red X); static resistive load (blue circle); and short circuit load (black star). The rectangular region denotes the approximate parameter space spanned by the DPWA shots; the relatively large parameter space is due to shot-to-shot variation in wire dynamics as well as in-shot inductance changes due to pinching.

figure include the inductance of adapting hardware that connects to the radial transmission line. For these simulations, the number of discrete transmission line elements N was set to 15, where each element represents a radius change dr of 3 cm with a transit time of 0.1 ns. With the radial transmission line gap height of 1.3 cm, impedances of the transmission line elements ranged from 0.96 Ω on the (large-radius) generator side to 2.32 Ω on the (small-radius) load side. Increasing N to values higher than 15 did not produce measurable differences in the load peak current or risetime for a variety of test cases.

Because the peak current and risetime contours in Figure 6 are nearly orthogonal, the time-averaged resistance and inductance for a given shot can be determined by finding the intersection of experimentally measured peak current and risetime. This procedure was performed for a sampling of previous MAIZE runs including planar foil,[25] cylindrical liner,[26] short-circuit, and resistive load shots, as indicated on the plots. For the dynamic load (planar foil and cylindrical liner) shots, the current pulses predicted from the combination of time-averaged inductance and resistance usually matched the observed current pulses to within a few percent, indicating that time-dependent behavior could be approximated as perturbations on the average parameters. The initial inductances for these loads were 8 nH (planar foil), 23 nH (cylindrical liner), 19 nH (short-circuit), and 12 nH (resistive load). These inductances generally agree with the time-averaged inductances observed in Figure 6; the larger variation in observed inductance on the short circuit load shots is attributed to arcing observed in the load region. While the time-averaged resistance of the dynamic loads exhibits more shot-to-shot variation, on average it is roughly half the pre-shot resistances (150 mΩ for planar foils and 50 mΩ for cylindrical liners).

The inductance-resistance parameter space for the DPWA loads used in the shots presented in this paper and in Ref. 7 is highlighted on the plot. The initial inductance of the DPWA loads, including the hardware adapting to the radial transmission line, was calculated to be 18 nH using ANSYS Maxwell. The inductance space includes an estimated uncertainty of 2 nH from the Maxwell simulation as well as the observed increases in inductance on DPWA shots (described in Section V) due to pinching. Time-averaged resistances were observed to range from approximately 50 mΩ to 70 mΩ for these shots.

It is noteworthy that peak current and risetime values for the DPWA shots on MAIZE presented in this paper and in Ref. 7 do not in general fit within the parameter space outlined in Figure 6. This discrepancy is due to an abnormally high firing delay in a large number of switches. On some shots, late firing switches extended the risetime and lowered the peak current; on others, arcing in the transmission line occurred, which artificially lowered the risetime observed by B-dot current monitors. These processes are described in detail in Sec. IV.

IV. EFFECTS OF SWITCH FIRING DELAY

In normal LTD operation, all spark-gap switches fire simultaneously to within their nominal jitter (usually less than 10 ns). However, these DPWA experiments were complicated by the fact that the LTD was nearing the end of a rebuild cycle, leading to many of the switches firing late or not at all. A switch timing diagnostic consisting of optical fibers connected to an array of photomultiplier tubes (PMTs) was fielded, with each optical fiber aimed at the trigger plane of a single switch. Up to 7 switches could be monitored on a single shot. Output signals from the photomultiplier tubes for a properly functioning switch and a poorly functioning switch are shown in Figure 7. The initial pulse occurs when the trigger gap breaks down, and the large spike in signal coincides with the switch becoming fully conductive, consistent with previous observations on these switches.[29] Each switch was monitored for five shots immediately after the DPWA campaign, giving a total of 200 switch timing measurements that were used to establish a model of switch firing timings. It was found that of the 40 switches, on each shot 14 ± 4 switches fired within 30 ns of the start of current, 8 ± 2 fired during the risetime of the current pulse, and 18 ± 6 fired after peak current had occurred. This diagnostic was also fielded on 4 random switches for each shot during the campaign to observe overall trends in switch behavior on the dynamic loads. The spread in switch firing times had dramatic effects on both the peak current and the shape of the current pulse and also introduced arcing in the transmission line. For a self magnetically insulated radial transmission line with $r \gg h$, where r is a radial position and h is the gap height, the magnetic cutoff condition can be approximated as

$$I_{cutoff}(r) > \frac{2\pi r}{\mu_0}\sqrt{\frac{2m_e V(r)}{eh^2}}, \tag{7}$$

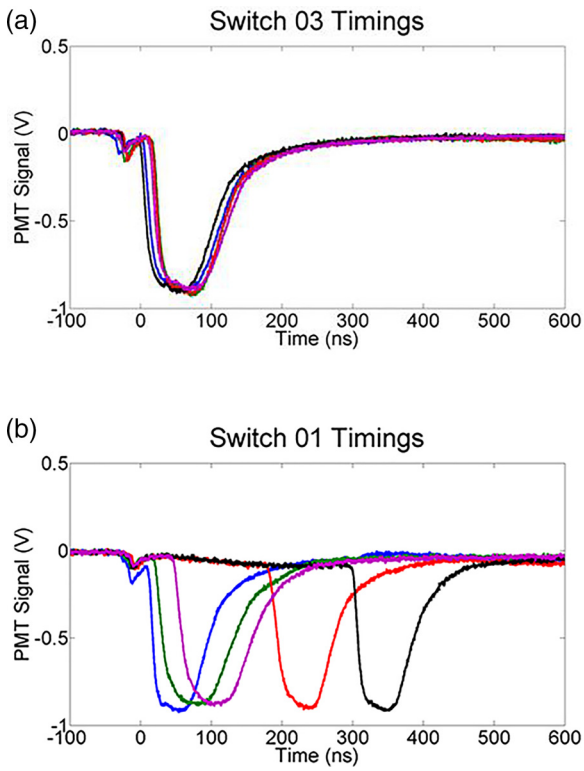

FIG. 7. Comparison of switch behavior over 5 consecutive shots into a static resistive load for (a) a properly functioning switch with approximately 10 ns jitter and (b) a malfunctioning switch with closing times ranging from 10 ns to 300 ns after nominal start of current.

where I_{cutoff} is the minimum current required for magnetic insulation, V is the voltage at a given radial position, and m_e, μ_0, and e are the mass of an electron, permeability of free space, and fundamental charge, respectively. If fewer switches fire on an LTD, the magnitude of the voltage pulse is largely unaffected, but the current will be lower, causing the outer portion of the radial transmission line to lose magnetic insulation and become vulnerable to arcing. Since the switch firing times were observed to be highly variable, a few shots had enough switches firing on time or during the risetime of the pulse to establish magnetic insulation, while other shots lost significant load current to arcs. Visible inspection of the transmission line confirmed that arcs occurred at a large radius that was outside the radius of the B-dot probe array. This allowed the presence or absence of arcs on a particular shot to be detected by the B-dots; on shots with arcing one or two of the B-dots showed a sharp drop in current early in the pulse, whereas on shots with no arcing all four B-dots integrated to give the same pulse shape.

Shots with arcing are virtually impossible to model from a circuit standpoint, as little information is available about the location, size, and conductivity of breakdown paths in the transmission line. Shots that exhibited significant pinching on the x-ray diagnostics were also the shots that did not exhibit arcing in the transmission line, which is expected as these shots had the highest current delivered to the load. Because the model implementation described in Section III assumes simultaneous switch firing, an additional circuit model was developed in LTSPICE treating each brick independently to account for the effects of switch firing time delays. In this model, the inductance and resistance of each brick are set to 40 times the lumped inductance and resistance of the generator section and the capacitance of each brick are set to 1/40th of the lumped capacitance represented in Figure 4. Switch trigger times are roughly estimated from the measurements described above. Time-averaged load resistance and fine adjustments to the trigger times are determined by matching the measured current pulse to the simulated current pulse early in time (up to approximately 150 ns after start of current, since the earliest observed pinch occurred after 200 ns) and late in time (at approximately 350 ns, just before spurious B-dot signals are expected). The initial load inductance was calculated using Maxwell and estimated assuming self-inductance dominates for the 12 parallel 5.1 μm diameter by 0.9 cm wires; both approaches gave 1.4 nH (regardless of interplanar spacing for the Maxwell calculation).

Time-dependent inductance of pinching DPWA loads is calculated by comparing measured current with output from the model using the initial load inductance. Because pinches and corresponding inductance changes were observed to occur near peak current on a timescale that is fast compared to the pulse length, the inductance change as a function of time is approximated by holding constant the stored energy $\frac{1}{2}LI^2$, where L represents the total inductance of the machine. Therefore, the difference between measured current and predicted current corresponds to a change in inductance.

Typical rates of inductance change during a pinch were of the order of 0.1–0.2 nH/ns. This rapid change generates a voltage pulse that propagates along the transmission line back to the switches. Near peak current, this voltage pulse is given by

$$V_{inductive} = L_{load}\frac{dI}{dt} + I\frac{dL_{load}}{dt} \approx I\frac{dL_{load}}{dt}, \tag{8}$$

where $V_{inductive}$ is the inductive voltage drop across the load and I is the current through the load. At peak currents near 400 kA the magnitude of this pulse often exceeded 50 kV. When this voltage pulse reached the switches, the untriggered switches immediately fired, sending a secondary current pulse into the load region. This behavior is supported by the PMT traces observed on shots with a successful pinch; switches that did not fire early in the current pulse all fired nearly simultaneously at a time corresponding to x-ray diode signals. This behavior exaggerated the current notches generally observed on pinches.

V. RESULTS FROM INDUCTANCE MEASUREMENTS AND DISCUSSION

Figure 8 shows current traces from the two shots with the most significant x-ray production of the campaign. Shot 937, shown in Figure 8(a), had an initial intergap spacing of 3 mm, and shot 938, shown in Figure 8(b), had an initial intergap spacing of 6 mm. The measured current is plotted along with predicted current from the circuit model described in Section IV using the 1.4 nH inductance of the initial solid-wire DPWA. Time-averaged resistance was found to be 65 mΩ for shot 937 and 50 mΩ for shot 938.

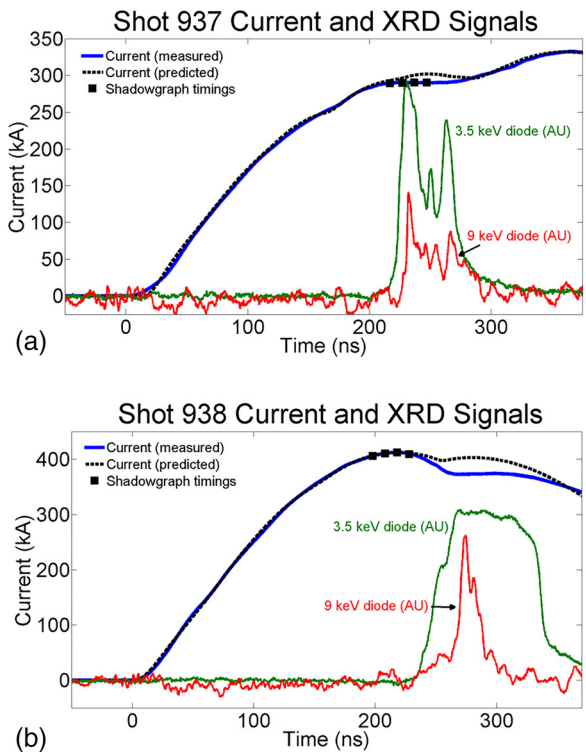

FIG. 8. Predicted and measured current traces from (A) shot 937 and (B) shot 938. Laser shadowgraph timings and signals from the x-ray diodes with filters of 3.5 keV and 9 keV in arbitrary units are also shown.

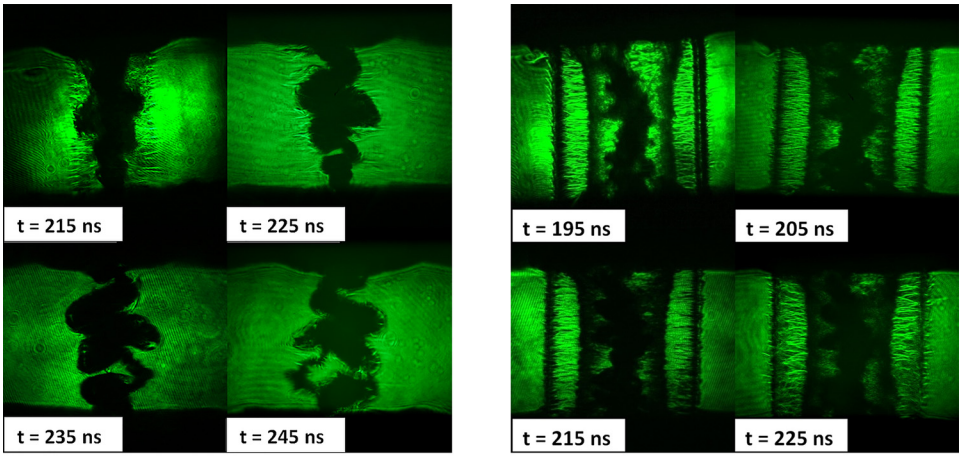

FIG. 9. Shadowgraph images from (a) shot 937 and (b) shot 938. Timing relative to start of current is indicated on each shadowgraph.

Signals from x-ray diodes with filters at 3.5 keV and 9 keV are shown on the same plot to give information on timings of the pinches (the 1.4 keV diode signals, not shown, made a prompt jump to saturation on both shots at approximately 220 ns and remained at the saturation value for several hundred ns). Timings from the four-frame shadowgraphy system are also indicated on the plots. These shadowgraphs are shown in Figure 9. For shot 937, the timing of the last shadowgraph occurs approximately at the peak of the pinch; for shot 938, the timing of the shadowgraphs lines up such that the latest image approximately captures the start of x-ray emission. From Figure 9(b), it is clear that a significant amount of mass still exists at the initial wire locations as late as 215 ns on the 6-mm gap DPWA, but between the 215 ns and 225 ns frames, much of this mass has transported to the central plasma. The last frame was captured approximately 50 ns prior to peak x-ray emission, as evident in Figure 8(b). The images from Figure 9(a) were captured during the pinch and show only a central plasma column. The qualitatively different implosion dynamics between the two shots are explained by the variation in aspect ratio, which is the ratio of the width of one of the wire planes to the intergap spacing. Shot 937 had a relatively high aspect ratio of 1.67, which produces an implosion that is characterized by the formation of a single precursor region, while shot 938 had a lower aspect ratio of 0.83, which produces an implosion that is characterized by both precursor formation and independent implosions of material from the two wire planes.

Figure 10 shows the load inductances calculated from the difference in predicted and measured current for these shots. The timings of the inductance change match quite well with x-ray emission observed on the x-ray diodes, and peak inductance occurs approximately halfway through the signals on the x-ray diodes. Additionally, the significantly larger inductance change observed on shot 938 corresponds with higher signal magnitudes on the x-ray diodes. This suggests the measurement of inductance change can provide information on both the timing and the strength of the pinch.

A minimum effective current-carrying diameter was determined from the magnitude of the inductance change for both shots, assuming that the self-inductance of the load region dominates over the mutual inductance with the return current posts. This diameter was found to be 3.0 mm for shot 937 and 1.0 mm for shot 938. Because the shadowgraphs from shot 938 captured an early time with considerable mass still at the initial wire positions, they did not provide an adequate comparison point to an estimate of a single pinch column, but fortunately the shadowgraphs from shot 937 occurred, while the pinch was in process. Figure 11 shows a close-up of the latest available shadowgraph from shot 937, which occurred within 5 ns of peak inductance. The 3.0 mm effective diameter is also shown in this figure. While the dramatic kink instability complicates the approximation of a single effective radius of current, the diameter of the central

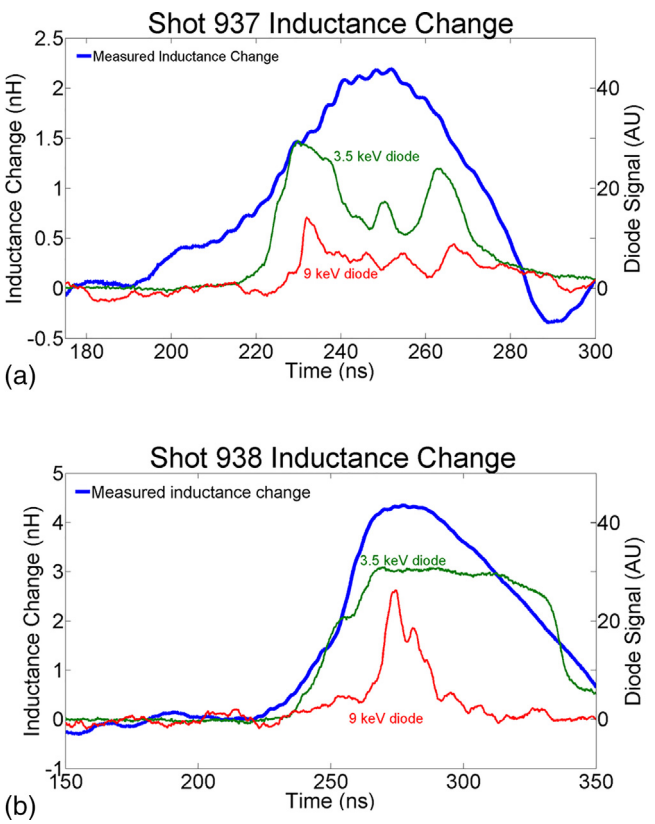

FIG. 10. Inductance change as a function of time for (a) shot 937 and (b) shot 938 (blue curves). Signals from the 3.5 keV (green) and 9 keV (red) x-ray are also shown. The timings of the inductance spikes agree very well with measurements of x-ray emission.

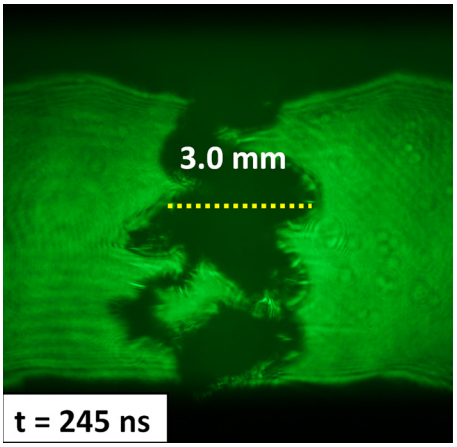

FIG. 11. Shadowgraph taken at approximate time of peak emission from shot 937. Effective current carrying radius calculated from the inductance change is also shown.

plasma column is on the order of the estimated current carrying diameter, indicating that the measurement is at least reasonable.

To provide a better evaluation of the ability of this method to measure average current-carrying radius, the method was applied to current measurements from cylindrical liner implosions[26] performed on MAIZE. These experiments utilized a 12-frame, ultrafast (5 ns minimum frame rate) intensified CCD with a single-beamline, repetitively split Nd:YAG pulse to provide up to 12 images per shot that include information from both laser shadowgraphy and plasma self-emission. As with the PWA experiments, time-dependent inductance of the load is calculated from the difference between measured current and predicted current and is used to determine current-carrying radius. The initial self-inductance of the aluminum liner for this shot was 2.4 nH, and the total load-side inductance including the adapter hardware for this load was found to be 23 nH using Maxwell. Time-averaged resistance was found to be 21 mΩ using Figure 6 for the observed peak current of 550 kA at 230 ns. Figure 12 shows the predicted and measured current for this shot. The plasma column diameter from each image is plotted against the time-dependent load inductance and calculated current-carrying diameter in Figure 13. Because the plasma-vacuum interface is unstable to the sausage, kink, and magneto Rayleigh-Taylor instabilities, the experimental plasma column diameter shown in Figure 13 represents a weighted average position of the interface, and the high and low error bars represent the plasma column at its thickest and thinnest points, respectively. Figure 13 demonstrates a remarkable agreement between the time-dependent calculated current-carrying diameter and the diameter of the plasma column visible on the shadowgraphs for all times except the latest available shadowgraph at t = 295 ns. The disagreement on the last frame is likely due to the assumption that that plasma resistance is constant, which may be violated late in time for a sufficiently strong pinch. The compression of the plasma column is expected to increase the temperature, which lowers the Spitzer-like plasma resistivity. If this decrease in resistance is non-negligible, it would lead to an underestimate of the inductance late in time, which explains the overestimate of current-carrying radius observed in the last frame. Self-emission observed on the CCD images supports this explanation; average CCD response measured in the plasma region on the 295 ns frame is approximately 15% higher than the response in the plasma region on the 235 ns frame.

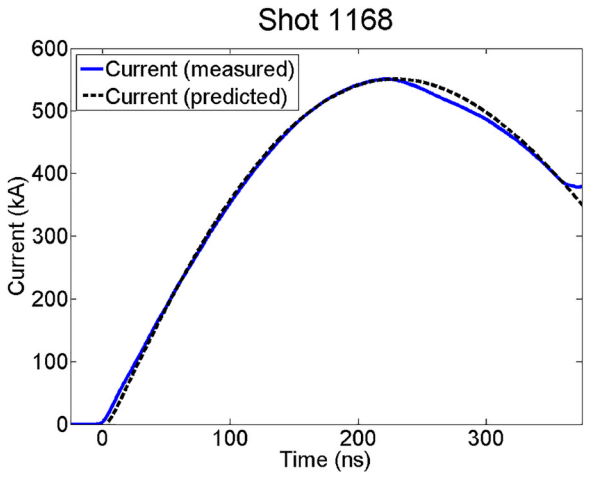

FIG. 12. Predicted and measured current traces for shot 1168, an implosion of an initially solid 400-nm aluminum liner.

Since the circuit model outputs voltage at all points in the system, the calculated voltage across the load could in principle be employed to estimate the energy coupled to the load, as was done in experiments on Saturn by Murphy *et al.*[23] and Comisso *et al.*[24] However, this analysis invokes the assumption that the load resistance is negligible, and in general our observed load resistances of 50–70 mΩ are of comparable impedance to the order-nH load inductances. Previous attempts to employ differential D-dot probes[30] to measure voltage on the MAIZE MITL have been unsuccessful due to prohibitively low signal-to-noise ratios; the high noise values are attributed to effects from the electron flow in the MITL. A voltage diagnostic that shows more promise for future experiments is the inductive voltage monitor (IVM) technique recently fielded on Z.[31] A similar IVM is

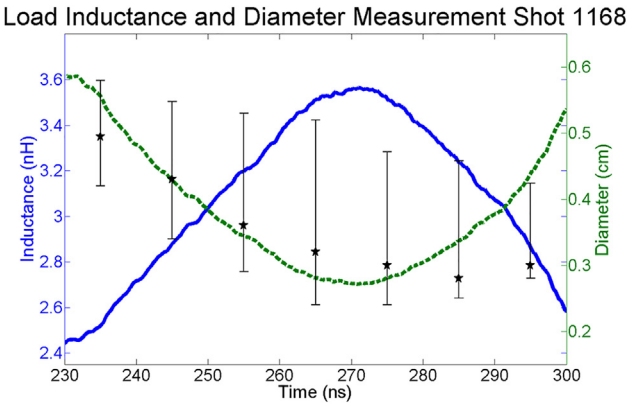

FIG. 13. Plasma column diameter measured from 10 ns-spaced framing camera images (stars) plotted against calculated current-carrying diameter (dashed curve) and load inductance (solid curve). Agreement between experiment and prediction is observed for all shadowgraph frames except the final frame at 295 ns. The error bars represent absolute upper and lower bounds on the plasma/vacuum interface diameter given by the plasma column at its thickest and thinnest point, respectively.

currently being developed for inclusion on future MAIZE experiments to enable measurements of coupled load energy.

VI. CONCLUSION

A circuit model for MAIZE was developed and implemented to measure the inductance change on DPWA implosions requiring only a current measurement as input. Because the switches were near the end of a rebuild cycle, they exhibited an unusually large closing time variation of several hundred nanoseconds. This required treating the circuit with a full, 40-brick model with independent switch firing times. The high switch jitter, combined with the natural load dependence of the low-impedance LTD, created load currents with substantially longer risetimes than observed on previous PWA experiments on Zebra.

The measured load inductance changes correlated well in time with x-ray emission on shots that exhibited significant pinching, indicating that the inductance measurement is a valid technique for determining pinch timing. The magnitude of the inductance change was also related to the signal measured by x-ray diodes with minimum energy thresholds of 3.5 keV and 9 keV. A minimum current-carrying radius also agreed qualitatively with a shadowgraph taken approximately halfway through the emitting portion of the pinch. Therefore, the inductance change magnitude can likely be used as a figure of merit describing the intensity of a pinching PWA plasma.

ACKNOWLEDGMENTS

This work was supported by the NNSA under DOE Cooperative Agreement No. DE-NA0001984, U.S. DoE Award No. DE-SC0012328, and Sandia National Labs. Sandia is a multiprogram laboratory operated by Sandia Corporation, a Lockheed-Martin company, for the United States Department of Energy's National Nuclear Security Administration under Contract No. DE-AC04-94AL85000. David Yager-Elorriaga is supported by an NSF fellowship under Grant No. DGE 1256260. The fast framing camera was supported by a DURIP, AFOSR #FA9550-15-1-0419.

[1]A. A. Kim, M. G. Mazarakis, V. A. Sinebryukhov, B. M. Kovalchuk, V. A. Visir, S. N. Volkov, F. Bayol, A. N. Bastrikov, V. G. Durakov, S. F. Frolov, V. M. Alexeenko, D. H. McDaniel, W. E. Fowler, K. LeChien, C. Olson, W. A. Stygar, K. W. Struve, J. Porter, and R. M. Gilgenbach, Phys. Rev. Spec. Top.-Accel. Beams **12**, 050402 (2009).

[2]M. G. Mazarakis, W. E. Fowler, A. A. Kim, V. A. Sinebryukhov, S. T. Rogowski, R. A. Sharpe, D. H. McDaniel, C. L. Olson, J. L. Porter, K. W. Struve, W. A. Stygar, and J. R. Woodworth, Phys. Rev. Spec. Top.-Accel. Beams **12**, 050401 (2009).

[3]R. M. Gilgenbach, M. R. Gomez, J. C. Zier, W. W. Tang, D. M. French, Y. Y. Lau, M. G. Mazarakis, M. E. Cuneo, M. D. Johnston, B. V. Oliver, T. A. Melhorn, A. A. Kim, and V. A. Sinebryukhov, AIP Conf. Proc. **1088**, 259 (2009).

[4]W. A. Stygar, M. E. Cuneo, D. I. Headley, H. C. Ives, R. J. Leeper, M. G. Mazarakis, C. L. Olson, J. L. Porter, T. C. Wagoner, and J. R. Woodworth, Phys. Rev. Spec. Top.-Accel. Beams **10**, 030401 (2007).

[5]W. A. Stygar, W. E. Fowler, K. R. LeChien, F. W. Long, M. G. Mazarakis, G. R. McKee, J. L. McKenney, J. L. Porter, M. E. Savage, B. S. Stoltzfus, D. M. Van De Valde, and J. R. Woodworth, Phys. Rev. Spec. Top.-Accel. Beams **12**, 030402 (2009).

[6]W. A. Stygar, T. J. Awe, J. E. Bailey, N. L. Bennett, E. W. Breden, E. M. Campbell, R. E. Clark, R. A. Cooper, M. E. Cuneo, J. B. Ennis, D. L. Fehl, T. C. Genoni, M. R. Gomez, G. W. Greiser, F. R. Gruner, M. C. Herrmann, B. T. Hutsel, C. A. Jennings, D. O. Jobe, B. M. Jones, M. C. Jones, P. A. Jones, P. F. Knapp, J. S. Lash, K. R. LeChien, J. J. Leckbee, R. J. Leeper, S. A. Lewis, F. W. Long, D. J. Lucero, E. A. Madrid, M. R. Martin, M. K. Matzen, M. G. Mazarakis, R. D. McBride, G. R. McKee, C. L. Miller, J. K. Moore, C. B. Mostrom, T. D. Mulville, K. J. Peterson, J. L. Porter, D. B. Reisman, G. A. Rochau, G. E. Rochau, D. V. Rose, D. C. Rovang, M. E. Savage, M. E. Sceiford, P. F. Schmit, R. F. Schneider, J. Schwarz, A. B. Sefkow, D. B. Sinars, S. A. Slutz, R. B. Spielman, B. S. Stoltzfus, C. Thoma, R. A. Vesey, P. E. Wakeland, D. R. Welch, M. L. Wisher, and J. R. Woodworth, Phys. Rev Spec. Top.-Accel. Beams **18**, 110401 (2015).

[7]A. S. Safronova, V. L. Kantsyrev, M. E. Weller, V. V. Shlyaptseva, I. K. Shrestha, M. Y. Lorance, M. T. Schmidt-Petersen, A. Stafford, M. C. Cooper, A. M. Steiner, D. A. Yager-Elorriaga, S. G. Patel, N. M. Jordan, R. M. Gilgenbach, and A. S. Chuvatin, IEEE Trans. Plasma Sci. **44**, 432 (2016).

[8]J. P. Chittenden, S. V. Lebedev, A. R. Bell, R. Aliaga-Rossel, S. N. Bland, and M. G. Haines, Phys. Rev. Lett. **83**, 100 (1999).

[9]R. D. McBride, T. A. Shelkovenko, S. A. Pikuz, D. A. Hammer, J. B. Greenly, B. R. Kusse, J. D. Douglass, P. F. Knapp, K. S. Bell, I. C. Blesener, and D. A. Chalenski, Phys. Plasmas **16**, 012706 (2009).

[10]V. L. Kantsyrev, A. S. Safronova, D. A. Fedin, V. V. Ivanov, A. A. Esaulov, V. Nalajala, I. Shrestha, S. Pokala, K. Williamson, N. D. Ouart, M. F. Yilmaz, P. Laca, T. E. Cowan, L. I. Rudakov, B. Jones, C. A. Coverdale, C. Deeney, P. D. LePell, A. L. Velikovich, and A. S. Chuvatin, IEEE Trans. Plasma Sci. **34**, 194 (2006).

[11]V. L. Kantsyrev, L. I. Rudakov, A. S. Safronova, D. A. Fedin, V. V. Ivanov, A. L. Velikovich, A. A. Esaulov, A. S. Chuvatin, K. Williamson, N. D. Ouart, V. Nalajala, G. Osbourne, I. Shrestha, M. F. Yilmaz, S. Pokala, P. J. Laca, and T. E. Cowan, IEEE Trans. Plasma Sci. **34**, 2295 (2006).

[12]V. L. Kantsyrev, L. I. Rudakov, A. S. Safronova, A. A. Esaulov, A. S. Chuvatin, C. A. Coverdale, C. Deeney, K. M. Williamson, M. F. Yilmaz, I. Shrestha, N. D. Ouart, and G. C. Osborne, Phys. Plasmas **15**, 030704 (2008).

[13]A. S. Safronova, V. L. Kantsyrev, A. A. Esaulov, N. D. Ouart, M. F. Yilmaz, K. M. Williamson, V. Shlyaptseva, I. Shrestha, G. C. Osborne, C. A. Coverdale, B. Jones, and C. Deeney, Rev. Sci. Instrum. **79**, 10E315 (2008).

[14]V. L. Kantsyrev, A. S. Safronova, A. A. Esaulov, K. M. Williamson, I. Shrestha, F. Yilmaz, G. C. Osborne, M. E. Weller, N. D. Ouart, V. V. Shlyaptseva, L. I. Rudakov, A. S. Chuvatin, and A. L. Velikovich, High Energy Density Phys. **5**, 115 (2009).

[15]K. M. Williamson, V. L. Kantsyrev, A. A. Esaulov, A. S. Safronova, P. Cox, I. Shrestha, G. C. Osbourne, M. E. Weller, N. D. Ouart, and V. V. Shlyaptseva, Phys. Plasmas **17**, 112705 (2010).

[16]A. S. Safronova, A. A. Esaulov, V. L. Kantsyrev, N. D. Ouart, V. Shlyaptseva, M. E. Weller, S. F. Keim, K. M. Williamson, I. Shrestha, and G. C. Osborne, High Energy Density Phys. **7**, 252 (2011).

[17]M. F. Yilmaz, A. S. Safronova, V. L. Kantsyrev, A. A. Esaulov, K. M. Williamson, I. K. Shrestha, M. E. Weller, G. C. Osbourne, and V. V. Shlyaptseva, High Energy Density Phys. **8**, 30 (2012).

[18]V. L. Kantsyrev, A. S. Chuvatin, A. S. Safronova, L. I. Rudakov, A. A. Esaulov, A. L. Velikovich, I. Shrestha, A. Astanovitsky, G. C. Osborne, V. V. Shlyaptseva, M. E. Weller, S. Keim, A. Stafford, and M. Cooper, Phys. Plasmas **21**, 031204 (2014).

[19]A. S. Safronova, V. L. Kantsyrev, A. A. Esaulov, A. S. Chuvatin, M. E. Weller, V. V. Shlyaptseva, I. Shrestha, S. F. Keim, A. Stafford, C. A. Coverdale, J. P. Apruzese, N. D. Ouart, and J. L. Giuliani, Phys. Plasmas **21**, 031205 (2014).

[20]M. E. Weller, A. S. Safronova, V. L. Kantysrev, A. A. Esaulov, I. Shrestha, J. P. Apruzese, J. L. Giuliani, A. S. Chuvatin, A. Stafford, S. F. Keim, V. V. Shlyaptseva, G. C. Osborne, and E. E. Petkov, Phys. Plasmas **21**, 031206 (2014).

[21]B. Jones, D. J. Ampleford, R. A. Vesey, M. E. Cuneo, C. A. Coverdale, E. M. Waisman, M. C. Jones, W. E. Fowler, W. A. Stygar, J. D. Serrano, M. P. Vigil, A. A. Esaulov, V. L. Kantsyrev, A. S. Safronova, K. M. Williamson, A. S. Chuvatin, and L. I. Rudakov, Phys. Rev. Lett. **104**, 125001 (2010).

[22]E. M. Waisman, M. E. Cuneo, W. A. Stygar, R. W. Lemke, K. W. Struve, and T. C. Wagoner, Phys. Plasmas **11**, 2009 (2004).

[23]D. P. Murphy, R. J. Allen, B. V. Weber, R. J. Commisso, J. P. Apruzese, D. G. Phipps, and D. Mosher, Rev. Sci. Instrum. **79**, 10E306 (2008).

[24]R. J. Commisso, J. P. Apruzese, J. Davis, S. L. Jackson, D. Mosher, D. P. Murphy, J. W. Thornhill, A. L. Velikovich, B. V. Weber, F. C. Young, J. S. Levine, B. H. Failor, H. Sze, N. Qi, J. W. Barrister, P. L. Coleman,

K. Wilson, M. Krishnan, C. A. Coverdale, B. Jones, and C. Deeney, in 7th International Conference on Dense Z-Pinches [AIP Proc. **1088**, 233 (2009)].
[25]J. C. Zier, R. M. Gilgenbach, D. A. Chalenski, Y. Y. Lau, D. M. French, M. R. Gomez, S. G. Patel, I. M. Rittersdorf, A. M. Steiner, M. Weis, P. Zhang, M. Mazarakis, M. E. Cuneo, and M. Lopez, Phys. Plasmas **19**, 032701 (2012).
[26]D. A. Yager-Elorriaga, A. M. Steiner, S. G. Patel, N. M. Jordan, Y. Y. Lau, and R. M. Gilgenbach, Rev. Sci. Instrum. **86**, 113506 (2015).
[27]M. G. Mazarakis, W. E. Fowler, K. L. LeChien, F. W. Long, M. K. Matzen, D. H. McDaniel, R. G. McKee, C. L. Olson, J. L. Porter, S. T. Rogowski, K. W. Struve, W. A. Stygar, J. R. Woodworth, A. A. Kim, V. A. Sinebryukhov, R. M. Gilgenbach, M. R. Gomez, D. M. French, Y. Y. Lau, J. C. Zier, D. M. VanDevalde, R. A. Sharpe, and K. Ward, IEEE Trans. Plasma Sci. **38**, 704 (2010).
[28]A. A. Kim, M. G. Mazarakis, V. I. Manylov, V. A. Vizir, and W. A. Stygar, Phys. Rev. Spec. Top-Accel. Beams **13**, 070401 (2010).
[29]J. R. Woodworth, J. A. Alexander, F. R. Gruner, W. A. Stygar, M. J. Harden, J. R. Blickem, G. J. Dension, F. E. White, L. M. Lucero, H. D. Anderson, L. F. Bennett, S. F. Glover, D. Van DeValde, and M. D. Mazarakis, Phys. Rev. Spec. Top.-Accel. Beams **12**, 060401 (2009).
[30]T. C. Wagoner, W. A. Stygar, H. C. Ives, T. L. Gilliland, R. B. Spielman, M. F. Johnson, P. G. Reynolds, J. K. Moore, R. L. Mourning, D. L. Fehl, K. E. Androlewicz, J. E. Bailey, R. S. Broyles, T. A. Dinwoodie, G. L. Donovan, M. E. Dudley, K. D. Hahn, A. A. Kim, J. R. Lee, R. J. Leeper, G. T. Leifeste, J. A. Melville, J. A. Mills, L. P. Mix, W. B. S. Moore, B. P. Peyton, J. L. Porter, G. A. Rochau, G. E. Rochau, M. E. Savage, J. F. Seamen, J. D. Serrano, A. W. Sharpe, R. W. Shoup, J. S. Slopek, C. S. Speas, K. W. Struve, D. M. Van De Valde, and R. M. Woodring, Phys. Rev. Spec. Top.-Accel. Beams **11**, 100401 (2008).
[31]E. M. Waisman, R. D. McBride, M. E. Cuneo, D. F. Wenger, W. E. Fowler, W. A. Johnson, L. I. Basilio, R. S. Coats, C. A. Jennings, D. B. Sinars, R. A. Vesey, B. Jones, D. J. Ampleford, R. W. Lemke, M. R. Martin, P. C. Schrafel, S. A. Lewis, J. K. Moore, M. E. Savage, and W. A. Stygar, Phys. Rev. Spec. Top.-Accel. Beams **17**, 120401 (2014).